Electronic Supplementary Material (ESI) for Journal of Materials Chemistry B.

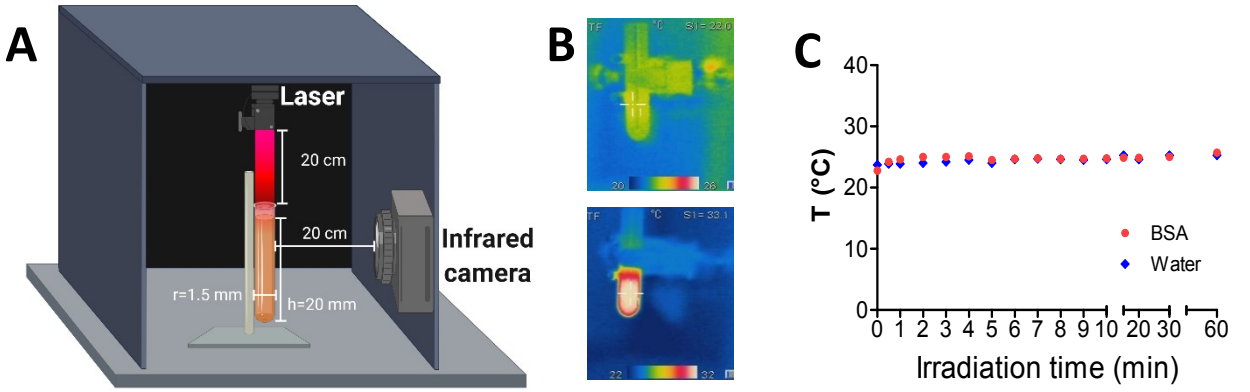

Supplementary 1. A. Description of the Irradiation system, laser output 0,350 W, Ø=3.5 mm, λ=808 nm. B. captured images of the infrared camera used for the temperature monitoring. C. Temperature increase of water and a BSA solution as blank control of irradiation, showing an insignificant temperature increase.

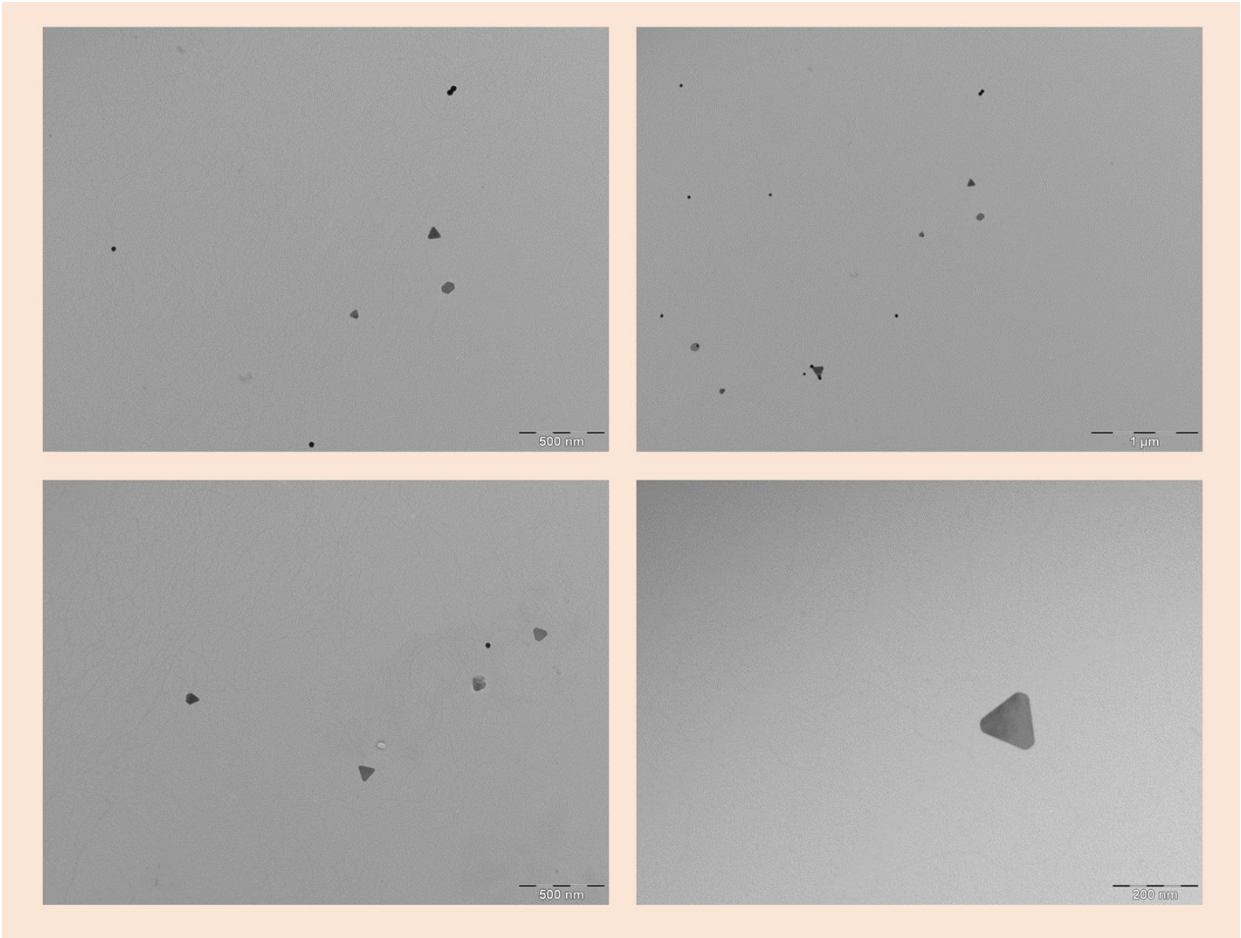

Supplementary 2. TEM images of AuNPrs after purification by centrifugation.

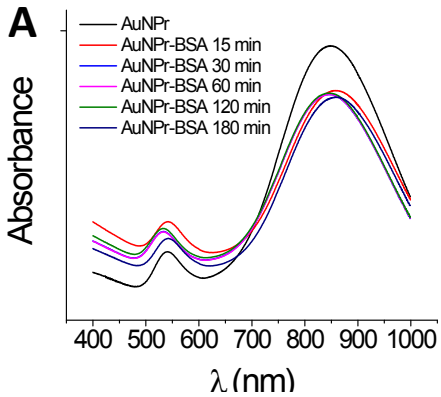

B	PDI	Pk 1 Mean Int	Pk 2 Mean Int	Z potential (mV)
AuNPrs	0,4	80±6	7±1	-27±0,2
AuNPr-BSA	0,4	93±12	11±1	-18±3

Supplementary 3. A. Uv-Vis spectrum of AuNPrs after interaction with BSA ([AuNPr]= 1 nmol L^{-1} [BSA]= 1000 mg L^{-1}) over time. B Hydrodynamic diameters and Z potential before and after protein corona formation.

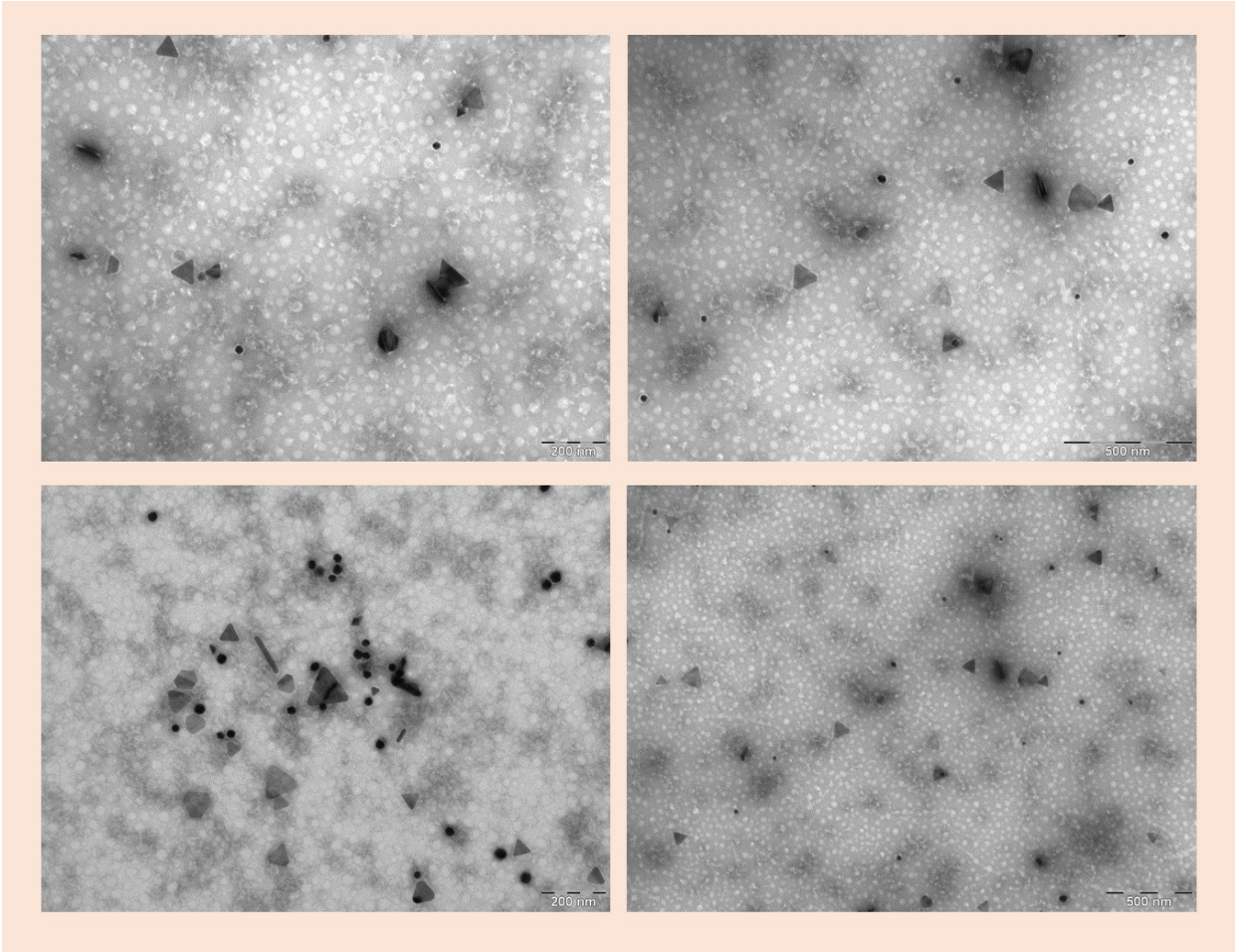

Supplementary 4. TEM images of AuNPrs after BSA coating.

Linear form	Plot
Freundlich isotherm $Log\ q_e = \frac{1}{n}\log C_e + \log K_F$	Log C_e vs log q_e
Langmuir isotherms	
Type I : $\frac{C_e}{q_e} = \frac{1}{q_m}\left(\frac{1}{K_L}\right) + \frac{C_e}{q_m}$	C_e vs $\frac{C_e}{q_e}$
Type II : $\frac{1}{q_e} = \frac{1}{q_m} + \left(\frac{1}{q_m K_L}\right)\frac{1}{C_e}$	$\frac{1}{C_e}$ vs $\frac{1}{q_e}$
Type III : $q_e = q_m - \left(\frac{1}{K_L}\right)\frac{q_e}{C_e}$	$\frac{q_e}{C_e}$ vs q_e
Type IV : $\frac{q_e}{C_e} = K_L q_m - K_L q_e$	q_e vs $\frac{q_e}{C_e}$
Kinetic models	
Pseudo 1st order: $\ln(q_e - q_t) = \ln(q_e) - k_1(t)$	*Time* vs $(q_e - q_t)$
Pseudo 2nd order: $\frac{t}{q_t} = \frac{t}{q_e} + \frac{1}{K_2 q_e^2}$	*Time* vs $\frac{t}{q_t}$

Supplementary 5. Langmuir and Freundlich isotherms and kinetic models linear equations. C_e represents the BSA concentration at equilibrium, q_m is the number of moles of BSA required to form a monolayer on one gram of AuNPs, q_e is the adsorption capacity, t is the time, K_F and K_L are the Freundlich and Langmuir constants, respectively. K_1, k_2 and k_i are the pseudo first and second order kinetic constants.

Supplementary 6. Calculation of the type of adsorption and surface area of AuNPrs

A characteristic dimensionless constant is proposed for Langmuir isotherms, in order to examine the progression of adsorption, namely R_L, which is indicative of the type of adsorption of BSA on AuNPrs. For a favored adsorption process $0<R_L<1$; for unfavored adsorption $R_L>1$; for linear adsorption $R_L=1$ and reversible adsorption $R_L=0$. [1,2] R_L was calculated as follows:

$$R_L = \frac{1}{1 + K_L C_0} \quad (1)$$

Where C_o is the concentration of BSA at time 0 (1000 mg/L), and K_L is the Langmuir constant. For this study, K_L was calculated as $8.8*10^{-4}$ L mg^{-1}; hence, the R_L value is 0.5, suggesting favored adsorption process of BSA on AuNPrs. [15] Additionally, essential parameters such as surface area (S_{NPr}) and monolayer saturation capacity q_m (i.e., the BSA maximum mass present in a monolayer upon AuNPrs) was calculated from the Langmuir adsorption model. The specific surface area in $m^2\ g^{-1}$ of AuNPrs is calculated as follows:[3]

$$S_{NPr} = \frac{q_m\ x\ a_{BSA}\ x\ N_A\ x\ 10^{-21}}{M} \quad (2)$$

Where q_m is the mass of BSA adsorbed in a monolayer, calculated as the inverse of the slope for Langmuir linear regression in figure 5, q_m= 47.6 mg g^{-1}, a_{BSA} is the occupied surface area of one molecule of BSA = 56 nm^2, [4] NA is the number of Avogadro 6.022 x 10^{23} mol^{-1}, and M is the molecular weight of BSA = 66463 g mol^{-1}. By replacing the values in the equation, a surface area of 24.2 $m^2\ g^{-1}$ was estimated.

Supplementary 7. Theoretical estimation of the occupation density of BSA on AuNPrs

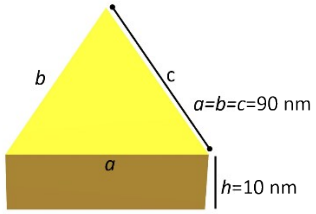

For AuNPrs of 90 nm edge length, the surface area was calculated as the sum of the two triangular and the three rectangular faces, A_T and A_R as follows:

$$A_T = 2 * c^2 \frac{\sqrt{3}}{4} = 7015\ nm^2 \qquad A_R = (a + b + c) * h = 2700\ nm^2$$

And the total calculated surface area of AuNPr is 9715 nm^2. In addition, BSA dimensions are 14x4x4 nm, as it is presented in the supplementary 11 and reported in the literature[4]. BSA can be attached to the gold surface and aligned in side-on or end-on arrange, as it is presented in figure 11 a and b, respectively. In the scenario a, BSA occupied area is 54 nm^2, resulting in a maximal density of 180 BSA/AuNPr; meanwhile, in the case of end-on arrange, a BSA molecule occupies 16 nm^2, thus, the maximal density is 607 BSA/AuNPr in the first layer, without considering unfolding of the protein.

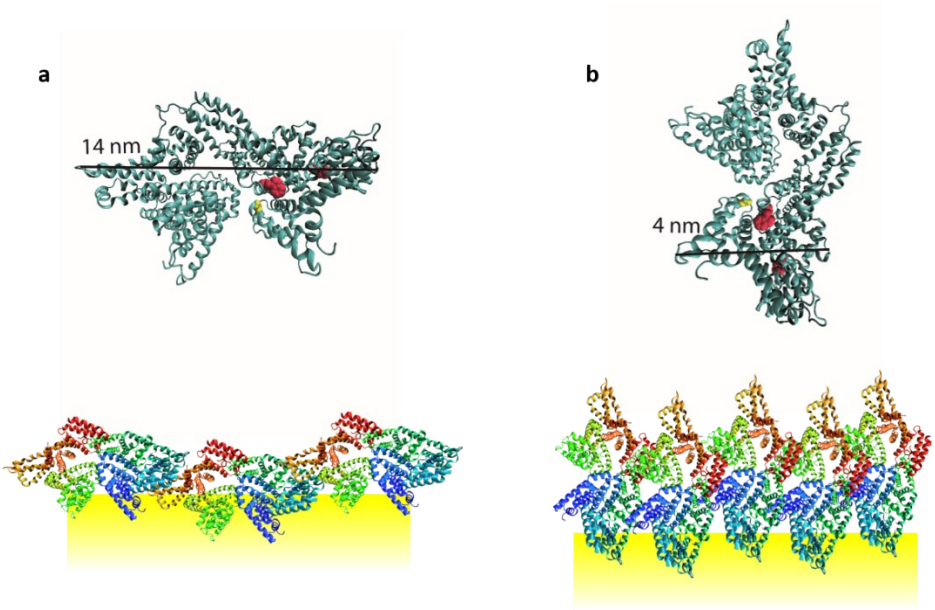

Supplementary 8. BSA size in nm and arrangement. A. aligned in side-on or b. end-on arrange

Supplementary 9. Calculation of thermodynamic parameters

As Maleki *et al*. proposed,[5] for the adsorption process in equilibrium, the thermodynamic equilibrium constant of adsorption was defined as:

$$K_0 = \frac{q_e}{C_e} \quad (3)$$

Where q_e and C_e are, the amount of BSA adsorbed at equilibrium time and the equilibrium constant, respectively. A linear plot between q_e and Ln (q_e/C_e) has the value of LnK_o as a vertical axis intercept (figure 7).

The Standard thermodynamic parameters, ΔG^0, ΔH^0 y ΔS^0, for the adsorption processes were defined as follows:[6,7]

$$\Delta G^0 = -RTlnK_0 \quad (4)$$

$$R\,T\,ln\,K_0 = T\Delta S^0 - \Delta H^0 \quad (5)$$

$$ln\,K_0 = -\frac{\Delta H^0 1}{R\ T} - \frac{\Delta S^0}{R} \quad (6)$$

The activation energy of the adsorption process can be calculated using the Arrhenius equation: [8]

$$Lnk_2 = Ln\,A - \frac{E_a}{R\,T}$$

Where k_2 is the pseudo-second-order rate constant (as it was described in adsorption kinetic parameters section), A is the Arrhenius factor, E_a the activation energy, and R the ideal gas constant (8.314 J/mol K). E_a is calculated by plotting ln k_2 vs. 1/T (figure 7).

The calculated values for the thermodynamic properties are presented in the following table:

Table 9.1. Values of thermodynamic parameters for the adsorption of BSA on AuNPrs

Temperature (K)	ΔG° (Jmol^{-1})	ΔH° (KJmol^{-1})	ΔS° (Jmol^{-1}K^{-1})	E_a (kJmol^{-1})
298	-3995.1 ± 396	-95.4 ± 21	-306.0 ± 69	45.7 ± 4
305	-2524.9 ± 228			
310	-212.4 ± 21			

Supplementary 10. Relative fluorescence change

Relative fluorescence change ($Q=(F_o-F)/F$) is an intrinsic property of the systems and determined for the number of binding sites in the protein. [11,12] The relationship between relative fluorescence and AuNPrs concentration, provide information about the number of binding sites in the protein, as well as the binding constant between AuNPs and BSA, from the Hill equation[13]:

$$log\left(\frac{F_0-F}{F}\right) = n * log[AuNP] + \log K$$

Where F_o and F are the fluorescence before and after the addition of AuNPrs, n is the Hill coefficient, *[AuNPr]* is the concentration of the AuNPr added, and K is the binding constant. By plotting $\log[(F_o-F)/F]$ vs. log[AuNP], n can be calculated as the slope of the following linear regression:

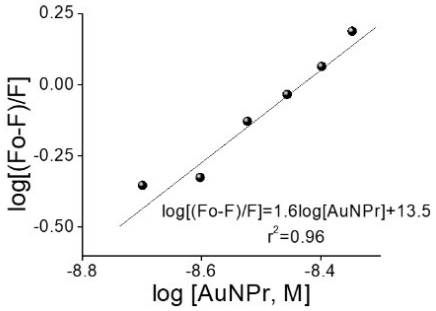

Supplementary 11. Logarithmic graph of relative fluorescence change after increasing concentrations of AuNPrs, from Stern-Volmer relationship

Hill coefficients are a measurement of cooperative binding and were calculated as 1.6±0.2 for AuNPrs. The predominant process is cooperativity binding, i.e., the binding of one BSA molecule on the AuNPrs surface increases the binding affinity of a second one at other sites of the receptor (AuNPrs).[14]

Supplementary 12

Using the data from the temperature increase profile over time upon laser irradiation (figure 11), the photothermal transduction efficiency, η_T, may be determined as follows: [9]

$$\eta_T = \frac{hA(T_{max} - T_{room}) - Q_0}{I(1 - 10^{A_\lambda})} * 100 \quad (7)$$

Where: h is the heat transfer coefficient; A is the cuvette surface area ($4.36*10^{-5}$ m^2); T_{max} and T_{room} corresponds to the highest temperature reached by every system and the room temperature, respectively; Q_0 is the energy contribution of the blank, calculated illuminating the system without AuNPrs[10] ($5.4*10^{-4}$ W, Supplementary 1); I is the intensity output of the laser (0.35 W), and A_λ is the absorbance of each nanoparticle´s solution at 808 nm.

For the determination of h, is applied the mass balance proposed by Roper *et al.*[9] First, a dimensionless driving force temperature, θ, is introduced, scaled using the maximum system temperature:

$$\theta = \frac{(T_{room} - T)}{(T_{room} - T_{max})} \quad (8)$$

A sample system time constant τ_s is assigned in the mass balance:

$$\tau_s = \frac{\sum_i m_i C_{p,i}}{hA} \quad (9)$$

Therefore, these two parameters (θ and τ_s), are related by the following equation:

$$\theta = e^{(\frac{-\theta}{\tau_s})} \quad (10)$$

Equation 10 can be solved by a linear regression of Ln(1-θ) vs. time, where τ_s= -1/slope of every linear equation (supplementary 8). After τ_s determination for each system, equation 9 solves for h, and the results are introduced in equation 7, for the determination of η_T. We have chosen the first five minutes for the linear regression of AuNPrs samples because it is the time of the more drastic temperature increase. Calculated photothermal efficiency of light to heat conversion on AuNPrs is η_T=32%; meanwhile, for AuNPrs-BSA is η_T=25%.

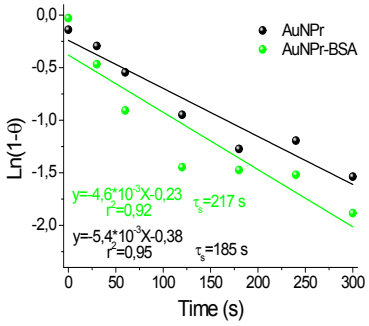

Supplementary 13. Calculation of τ_s for photothermal efficiency after NIR irradiation in continuous laser. Line regression of Ln (1-θ) vs time: AuNPr-PEG (black) and AuNPr-BSA (green).

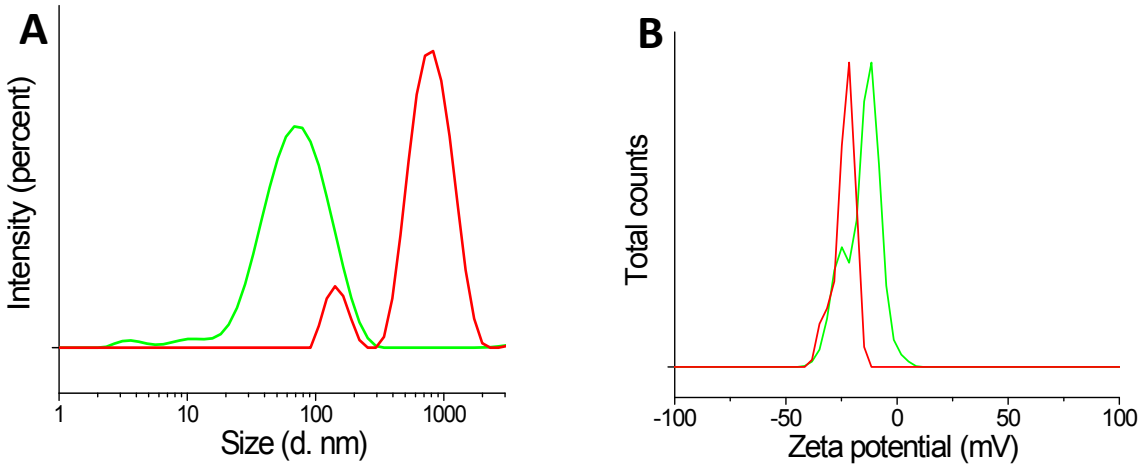

C	Pk 1 Mean Int	Pk 2 Mean Int	Z potential (mV)
AuNPrs-BSA	93±12	11±1	-18±3
AuNPr-BSA+NIR	894±20	120±5	-11±3

Supplementary 14. Aggregation effects after 15 min of 808 nm and 350 mW irradiation on: A. Hydrodynamic diameters and B. Z potential. C. summary of the results. Green line AuNPrs-BSA, red line AuNPrs-BSA after NIR irradiation

References:

1 S. Rahdar, A. Rahdar, S. Ahmadi and J. F. Trant, *Can. J. Chem.*, 2019, **97**, 577–583.

2 A. Mittal, L. Kurup and J. Mittal, *J. Hazard. Mater.*, 2007, **146**, 243–248.

3 A. Itodo, H. Itodo and M. Gafar, *J. Appl. Sci. Environ. Manag.*, 2011, **14**, 1–5.

4 H. T. M. Phan, S. Bartelt-Hunt, K. B. Rodenhausen, M. Schubert and J. C. Bartz, *PLoS One*, 2015, **10**, e0141282.

5 M. S. Maleki, O. Moradi and S. Tahmasebi, *Arab. J. Chem.*, 2017, **10**, 491–502.

6 R. T. M. Dharmendirakumar, G.Vijayakumar, G. Vijayakumar, R. Tamilarasan and M. Dharmendirakumar, *J. Mater. Environ. Sci.*, 2015, **3**, 157–170.

7 I. P. Mosiagin, A. D. Furasova, M. A. Kozlova, M. G. Osmolowsky and O. M. Osmolovskaya, *Russ. J. Gen. Chem.*, 2015, **85**, 2654–2656.

8 M. H. Çalımlı, Ö. Demirbaş, A. Aygün, M. H. Alma, M. S. Nas and F. Şen, *Appl. Water Sci.*, 2018, **8**, 1–12.

9 D. K. Roper, W. Ahn and M. Hoepfner, *J. Phys. Chem. C*, 2007, **111**, 3636–3641.

10 M. Almada, B. H. Leal-martínez, N. Hassan, M. J. Kogan, M. G. Burboa, A. Topete, M. A. Valdez and J. Juárez, *Mater. Sci. Eng. C*, 2017, **77**, 583–593.

11 P. B. Kandagal, S. Ashoka, J. Seetharamappa, S. M. T. Shaikh, Y. Jadegoud and O. B. Ijare, *J. Pharm. Biomed. Anal.*, 2006, **41**, 393–399.

12 A. G. Kozlov, R. Galletto and T. M. Lohman, *NIH Public Access*, 2012, **922**, 55–83.

13 S. P. Boulos, T. A. Davis, J. A. Yang, S. E. Lohse, A. M. Alkilany, L. A. Holland and C. J. Murphy, *Langmuir*, 2013, **29**, 14984–14996.

14 J. Mariam, S. Sivakami and P. M. Dongre, *J. Biomol. Struct. Dyn.*, 2017, **35**, 368–379.